ACS central science

Research Article

http://pubs.acs.org/journal/acscii

Nucleic Acid Templated Chemical Reaction in a Live Vertebrate

Laurent Holtzer, Igor Oleinich, Marcello Anzola, Eric Lindberg, Kalyan K. Sadhu, Marcos Gonzalez-Gaitan,* and Nicolas Winssinger*

School of Chemistry and Biochemistry, NCCR Chemical Biology, University of Geneva, 30 quai Ernest Ansermet, Geneva, Switzerland

Supporting Information

ABSTRACT: Nucleic acid templated reactions are enabled by the hybridization of probe-reagent conjugates resulting in high effective reagent concentration and fast chemical transformation. We have developed a reaction that harnesses cellular microRNA (miRNA) to yield the cleavage of a linker releasing fluorogenic rhodamine in a live vertebrate. The reaction is based on the catalytic photoreduction of an azide by a ruthenium complex. We showed that this system reports specific expression of miRNA in living tissues of a vertebrate.

The ability to perform bio-orthogonal chemical transformations in a live organism has empowered chemical biology and enabled methods to report on complex biochemical events.[1] To date, only a handful of reactions with abiotic partners and orthogonal reactivity to native cellular components have been reported for *in vivo* chemical transformations.[2] Herein we report the use of a ruthenium-catalyzed azide reduction to visualize in a time-controlled manner the expression of specific microRNAs (miRNA) in a live vertebrate based on a sequence specific templated reaction.

Life is orchestrated by a biomolecular circuitry arising from genetic information. miRNAs have emerged as important regulators in these genetic circuitries with implications in cellular differentiation and numerous pathologies.[3,4] It is estimated that 20−30% of all human genes are partially regulated by miRNAs.[5] The ability to visualize specific regulatory miRNAs in an organism is quintessential for biological and biomedical research. *In situ* hybridization methods are most often used to detect mRNA or miRNA in fixed cells, tissues, or whole embryos.[6] The pursuit of technologies amenable to nucleic acid sensing in live cells has led to the development of molecular beacons,[7] nanoflares,[8] cascade hybridization reactions,[9] and templated chemical reactions.[10,11] Notwithstanding landmark accomplishments in live cells, none of these methods have yet succeeded in detecting specific nucleic acid sequences in live vertebrates. The present work builds upon a previous study in HeLa cells.[12] However, it is important to validate that this technology works in a model organism: imaging RNA in zebrafish by our method opens the possibility to study the role of genes (in particular microRNAs; miRNA) during development, which is not accessible with culture cells like HeLa. The usage in a vertebrate model organism is not trivial, and a number of challenges had to be addressed: (1) the reagents must be stable over at least 24 hpf in a live animal, (2) the process must be sufficiently efficient to work following some dilution upon cell proliferation during embryonic growth, (3) the reagents must show low toxicity to be administered at sufficiently high concentrations, and (4) the reaction itself must be compatible with the embryonic development in a living animal.

Nucleic acid templated reactions rely on the close proximity of reagents achieved upon hybridization of reagent−probe conjugates to promote the reaction.[13] We developed a method which is based on the photoexcitation of the ruthenium catalyst[14] which reduces the vicinal azide. This reduction, in turn, leads to immolation of the linker through 1,6-eliminations thus unmasking a fluorogenic rhodamine (Figure 1a,b).[12] It has been shown that conversions exceeding template loading were obtained through turnover on the template. At low template loading (high excess of reagents), an amplification of >4000-fold was obtained over 24 h.[12] The fact that the reaction requires external light (455 nm) makes the system suitable for temporal and spatial control by applying external light when and where desired. While injection of the probe is performed at the onset of zebrafish embryogenesis (unicellular stage), the metabolic stability of PNA[15] coupled to the temporal control of this Ru-based templated reaction raises the possibility of detecting specific nucleic acid sequences at a later time during embryogenesis (Figure 1c).

We first investigated the distribution of the probe using the fluorescence emission at 600−640 nm of the ruthenium complex (imaged using time-gated confocal fluorescence microscopy). We studied three of the different PNA probes, which were injected into one-cell-stage embryos. Figure 2a illustrates that control embryos show 600−640 nm autofluorescence of the yolk. Beyond the yolk, the ruthenium−PNA conjugates are distributed homogeneously in the rest of the body, indicating that the PNA probes do not show by themselves a bias in their localization (see Figure 2b for a representative example). No apparent toxicity was observed in the injected embryos. This is consistent with the fact that PNAs

Received: February 29, 2016
Published: May 18, 2016

DOI: 10.1021/acscentsci.6b00054
ACS Cent. Sci. 2016, 2, 394−400

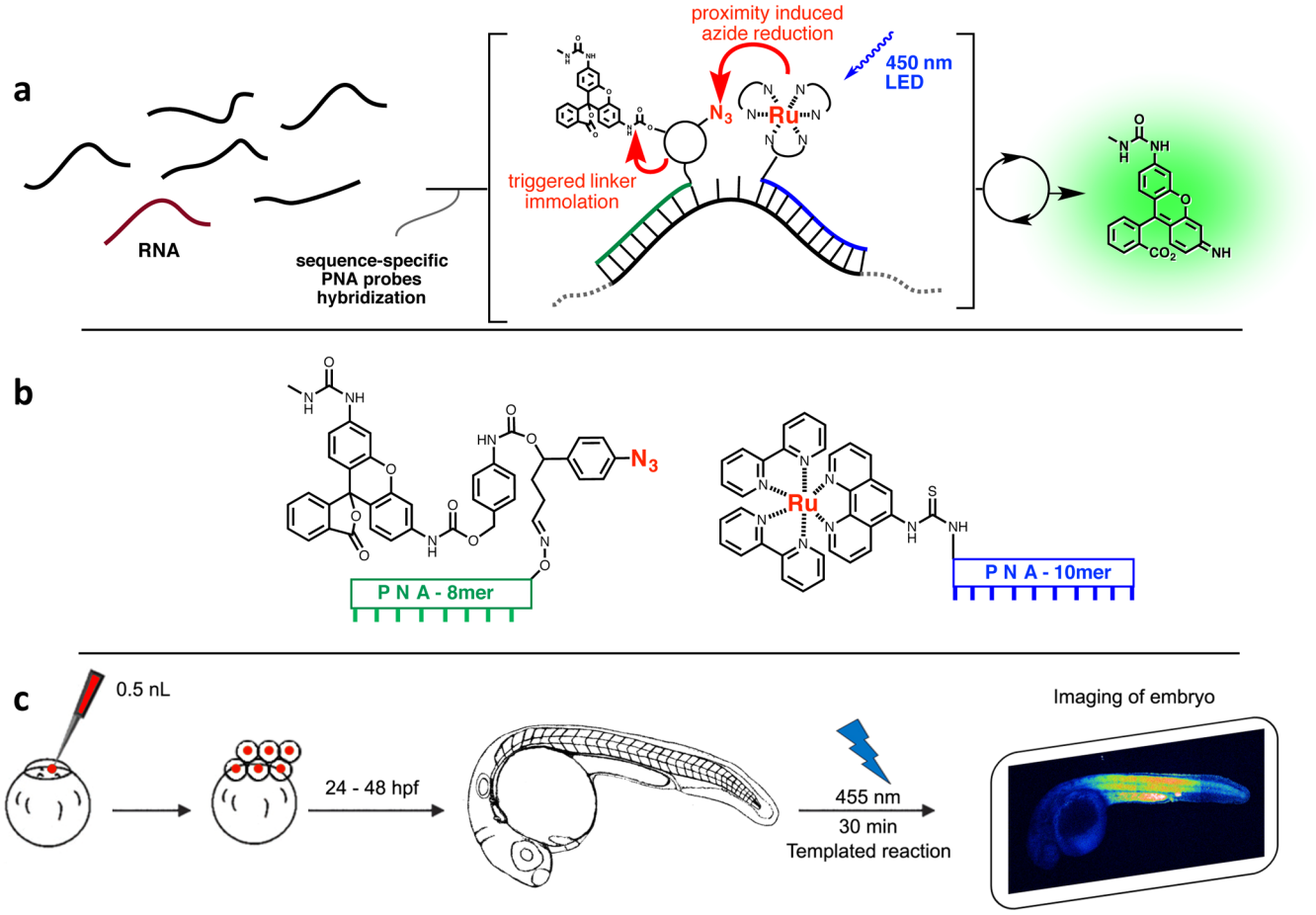

Figure 1. miRNA templated reaction. (a) Schematic representation of the sequence-specific nucleic acid templated reaction. (b) Chemical structure of the reacting partners. (c) Schematic representation of the protocol: The probe set is injected into one-cell-stage embryos. Embryos are immediately placed in the dark at 28 °C to prevent the templated reaction. At the stage of interest, embryos are exposed to blue light (λ = 455 nm) for 30 min, placed into 1.0% low melting point agarose in 0.3× Danieau, and anesthetized with tricaine. Fluorescence imaging is done using a 20× 1.0 NA water-dipping objective on a Zeiss LSM710 upright confocal microscope.

only show antisense effects through steric blocking and the PNAs used are too short to achieve efficient steric blocking of miRNA hybridization or mRNA translation.

We next designed and validated PNA probes for three different miRNAs that are expressed in a tissue specific fashion at various stages of development.[16] miR-9 is associated with neuronal development: it has been reported[16,17] to be specifically present in the brain at 24 hpf (Figure 2g[16]) and extends to the spinal cord at 36 hpf (Figure 2h[16]). miR-196 (our probe combination is specific for miR-196a, c and d) has been implicated in the establishment of the body axis, during the development of the tail and the pectoral fin and during regeneration.[18,19] At 24 hpf, it is present at the distal tip of the tail (Figure 2i[16]). miR-206 regulates the patterned expression of specific muscle genes, promotes muscle differentiation,[20] controls the levels of VegfA in muscle,[21] and is present in the head and body muscles at 24 hpf (Figure 2j[16]).

Mature miRNAs are difficult to detect using standard *in situ* hybridization protocols owing to their short length (20−23 nucleotides) and thereby require the usage of LNA probes[22] as well as additional cross-linking steps to avoid miRNA diffusion out of cells during the long incubation and washing steps.[23] However, these short sequence stretches are not a limitation for templated reactions using PNA probes since efficient reactions are achieved with reagents tethered to 8−11mer probes. We designed our probes as 8−11mer, so that hybridization is very transient and it does not lead to silencing. Indeed the probes do not affect localization nor function of the RNA as judged by its comparison by other methods. If a longer probe is used (23mer), miRNA silencing has been reported.[24] The design of the probes includes a modification at the γ-position of the PNA backbone at alternating positions which is known to enhance the specificity of hybridization while increasing aqueous solubility[25,26] (see Supporting Information for exact structure of probes). For each target sequence, a perfect match (PM) rhodamine conjugate and a mismatch rhodamine conjugate (MM; sequence with two nucleobases mismatch as negative control) were used with the same ruthenium conjugate in the reactions. The sequence specificity of each reaction was tested by doing *in vitro* kinetic measurements on a synthetic template (Figure 2d−f).

The PNA probes were injected (for miR-9 and miR-196: 0.5 nL of a solution containing the Ru conjugate (125 μM) together with the fluorogenic rhodamine conjugate (500 μM); for miR-206 concentrations were halved) into the cell (and not the yolk) of one-cell-stage wild-type zebrafish embryos. Embryos were subsequently raised in the dark at 28 °C. At 24 hpf or 36 hpf, the embryos were exposed to 455 nm light using a 1 W LED lamp for 30 min. To immobilize embryos for subsequent imaging, live embryos were then placed into 1%

DOI: 10.1021/acscentsci.6b00054
ACS Cent. Sci. 2016, 2, 394−400

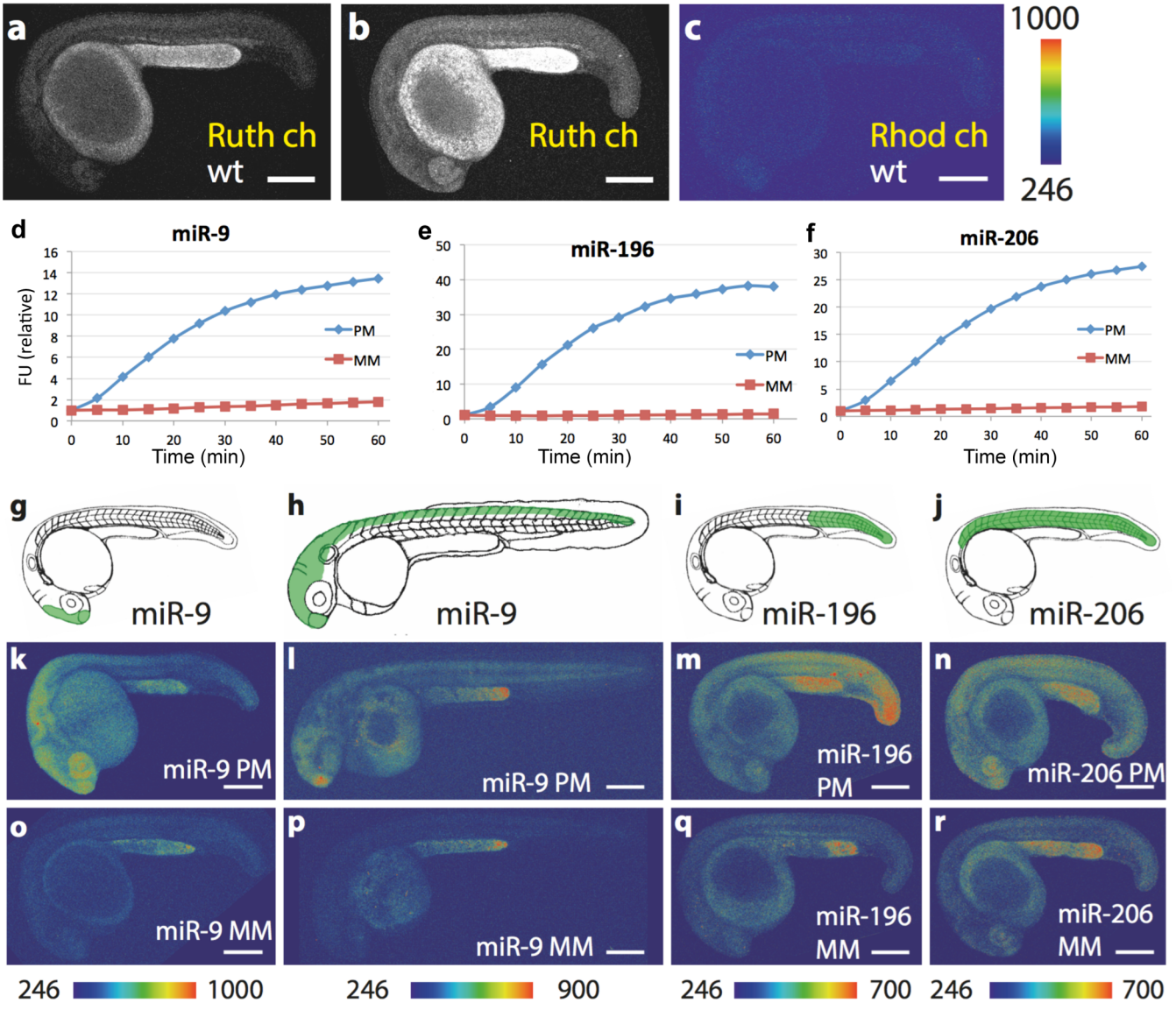

Figure 2. *In vivo* miRNA templated chemistry. Identification of miRNA localization in 24 hpf or 36 hpf zebrafish embryos using confocal microscopy. Wild-type zebrafish embryos were injected with 0.5 nL of a mixture of appropriate Rho-PNA and Ru-PNA probes (ratio 4:1). (a) Representative image of a nontreated embryo (wild type) in the ruthenium channel. (b) Ru-PNA-only injected embryo in the ruthenium channel. (c) Representative image of a nontreated embryo (wild type) in the rhodamine channel. (d–f) Kinetics of the templated reaction on synthetic DNA template for each miRNA using PM and MM probe combinations (reactions performed with 250 nM of rhodamine probe, 20% ruthenium probe, and 20% template). (g–j) Scheme of zebrafish embryos indicating the location of miRNA expression. (k–r) Maximum intensity projections of image stacks showing rhodamine fluorescence in live zebrafish embryos injected with either matched probes (PM: k–n) or mismatched probes (MM: o–r) after 30 min of irradiation with 455 nm light. Images were assembled from tile scans using ImageJ. Color lookup tables (LUTs) are identical for each PM–MM pair and shown below each pair. Scale bar = 250 μm.

low-melting agarose in 0.3× Danieau and anesthetized with 0.020% tricaine (see Supporting Information). Embryos were imaged on an upright confocal microscope. Under our conditions of imaging, uninjected control embryos show a negligible background signal (Figure 2c).

As shown in Figure 2k–r, each set of PM probes yielded a distinct fluorescent pattern consistent with the reported tissue-specific expression of the target sequence,[16,27] while the corresponding MM showed a homogeneous, low intensity signal. The fluorescence intensity was quantified by calculating the average within a rectangular area of approximately 10–40 cells in a specific tissue considering the maximum intensity projection of an image stack. The measured intensities were plotted for different regions along the anterior–posterior axis of the embryos, as shown in Figure 3 (see Figures S1–S6 for images of individual embyos). We observed variations in the absolute fluorescence intensity across the different embryos for the miRNA considered, which is likely due to variability in injection volume and/or to interembryo variability in the level of expression.

For miR-9 at 24 hpf, a brain-specific increase in fluorescence I was observed in 8 out of 10 embryos when comparing brain vs tail (I_{brain} = 623 ± 49; I_{tail} = 462 ± 31; Figure 3a), while much lower differences can be detected in the group treated with the corresponding MM probes (I_{brain} = 317 ± 10; I_{tail} = 306 ± 12; Figure 3a). The brain/tail fluorescence ratio is significantly increased when comparing PM treated embryos with MM treated (ratio$_{PM}$ = 1.37 ± 0.10; ratio$_{MM}$ = 1.07 ± 0.03; Figure

DOI: 10.1021/acscentsci.6b00054
ACS Cent. Sci. 2016, 2, 394–400

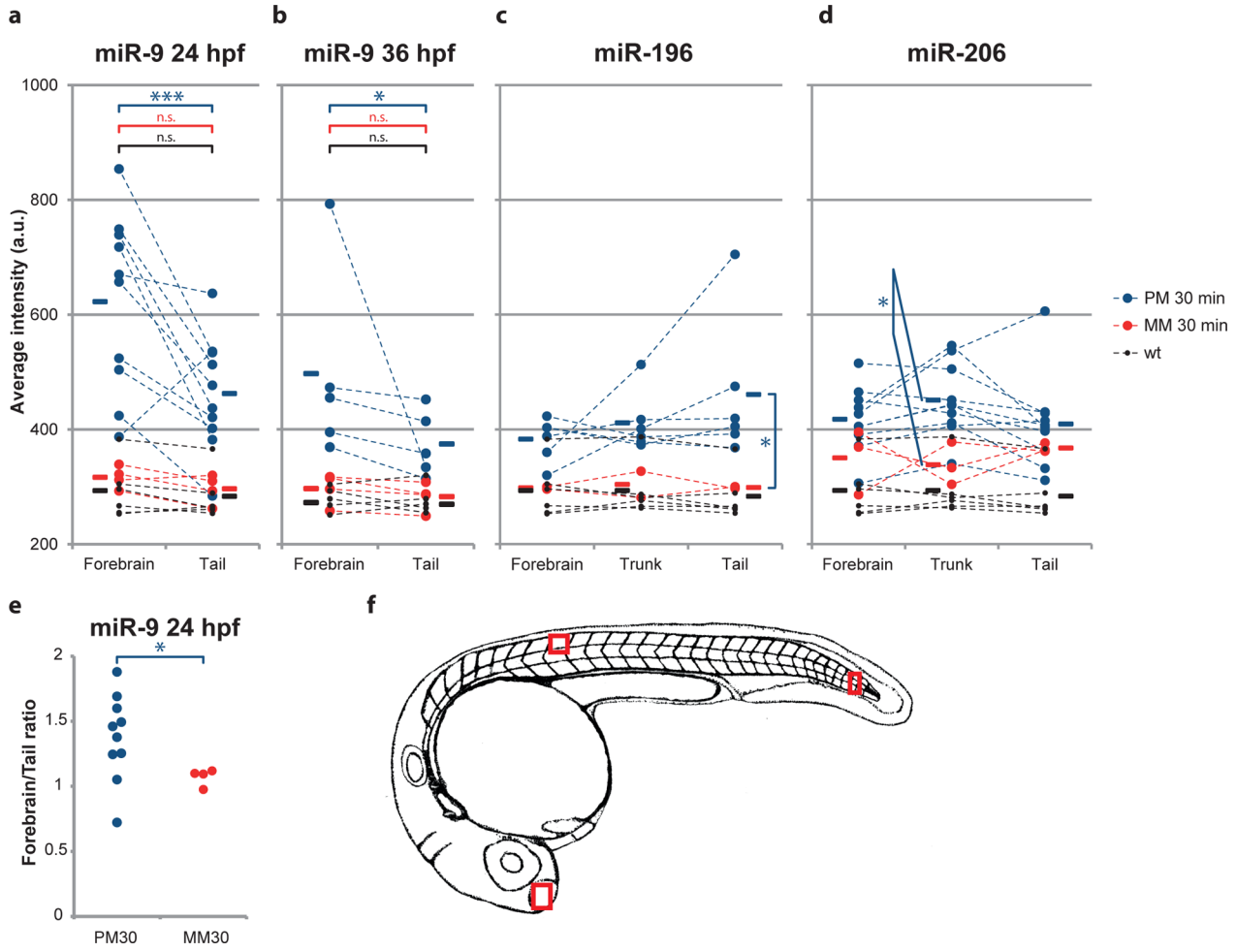

Figure 3. Fluorescence intensities measured at different locations in individual embryos for all studied miRNA targets after 30 min of templated chemistry. (a–d) Average fluorescence intensity across a representative area of the tissue (10–40 cells) in PM-treated embryos (blue), MM-treated embryos (red), and untreated embryos (black). Mean fluorescence intensity (indicated by horizontal bars) is higher in PM treated embryos compared to MM treated embryos or noninjected embryos. For miR-196 (tail) and miR-206 (trunk) statistical significance is shown (one-tailed Mann–Whitney test; miR-196, PM (n = 6), MM (n = 2); miR-206, PM (n = 9), MM (n = 3)). Images of individual embryos are shown in Figures S1–S6; (a, b) Fluorescence intensity in the forebrain is significantly higher than intensity in the tail for miR-9 24 hpf and 36 hpf (one-tailed paired Wilcoxon test; miR-9 24 hpf, PM (n = 10), MM (n = 4); miR-9 36 hpf, PM (n = 5), MM (n = 4)). (e) Brain/tail fluorescence ratio in miR-9 24 hpf embryos is significantly higher for PM treated embryos compared to MM treated embryos (one-tailed Mann–Whitney test). (f) Red boxes indicate which areas of the tissue were used for average intensity measurements.

3e). Performing the same experiment at 36 hpf (PM, I_{brain} = 497 ± 76, I_{tail} = 374 ± 26; MM, I_{brain} = 297 ± 14, I_{tail} = 283 ± 12; Figure 3b) also shows differences between the brain and the tail, although the differences are smaller than at 24 hpf, consistent with previously reported *in situ* images[16]. Significantly, the group treated with PM probes consistently afforded higher signal than the group treated with MM probes.

In the case of miR-196 (Figure 3c), the group treated with PM probes consistently yielded higher signal than the group treated with MM probes. Furthermore, in embryos showing high fluorescent intensity (n = 2), the signal is stronger in the tail than in the head. It should be noted that the different miR-196 genes are expressed at different stages in development and that their patterns differ from each other at 24 hpf.[16] The combined expression levels of these genes might therefore be quite sensitive to the developmental stage. Thus, the observed interembryo variability may be a result of slight differences in the developmental stages used in our experiments. Finally, in the case of miR-206 (Figure 3d), a general higher fluorescence intensity is observed for the PM probes vs MM probes with a maximum in the trunk of the embryo. Images of individual embryos are shown in Figures S1–S6. As expected, MM treated embryos showed a slight increase in fluorescence compared to uninjected embryos (shown in black in Figure 3a–d), caused by background fluorescence and reaction.

Treated embryos survived until at least 5 dpf (maximum duration of the protocol) and did not display any morphological phenotypes. We observed a slight growth delay probably caused by the injection procedure itself. The viability and the lack of observable phenotypes of embryos having undergone a templated reaction for up to 4 days post reaction suggest that the reaction does not cause major toxicity.

The reaction parameters were further investigated to test the qualitative impact of variation in the injection volume or probe ratio. We focused on the probes for miR-9 (which yielded a distinct localization in the brain (Figure 2g,k; Figure 3a) consistent with what was reported previously.[16] The performance of the *in vitro* reaction was investigated using a fixed template loading (20%) but different overall concentration (250 nM to 10 nM of rhodamine probe). As shown in Figure

DOI: 10.1021/acscentsci.6b00054
ACS Cent. Sci. 2016, 2, 394–400

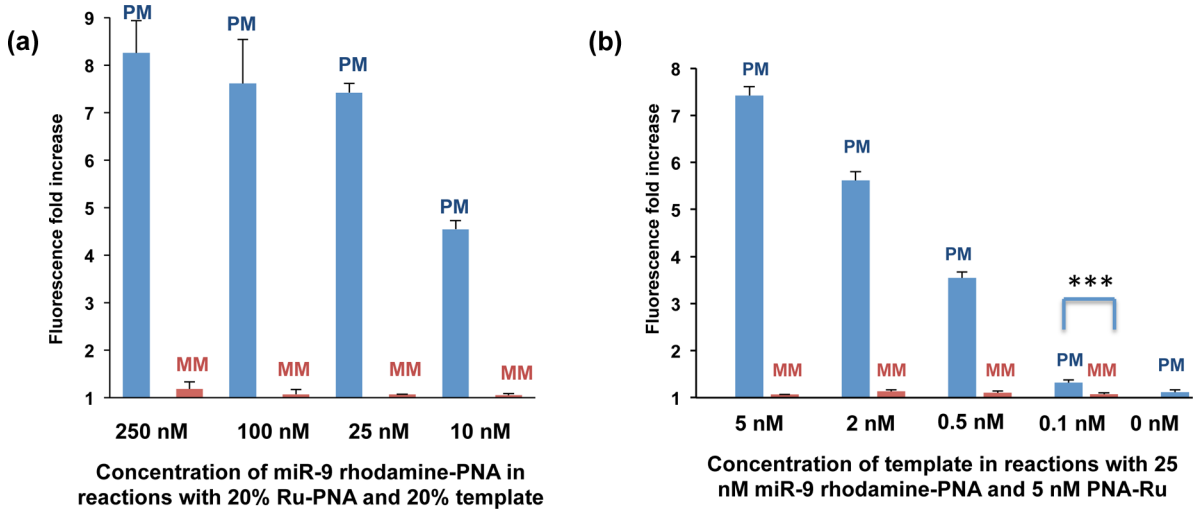

Figure 4. Templated reaction using synthetic DNA template (miR-9). (a) End point measurements of fluorescence increase (30 min irradiation) for reactions performed with the same ratio of reagents but different overall concentration. (b) End point measurement of fluorescence increase (30 min irradiation) for reactions performed with decreasing template loading.

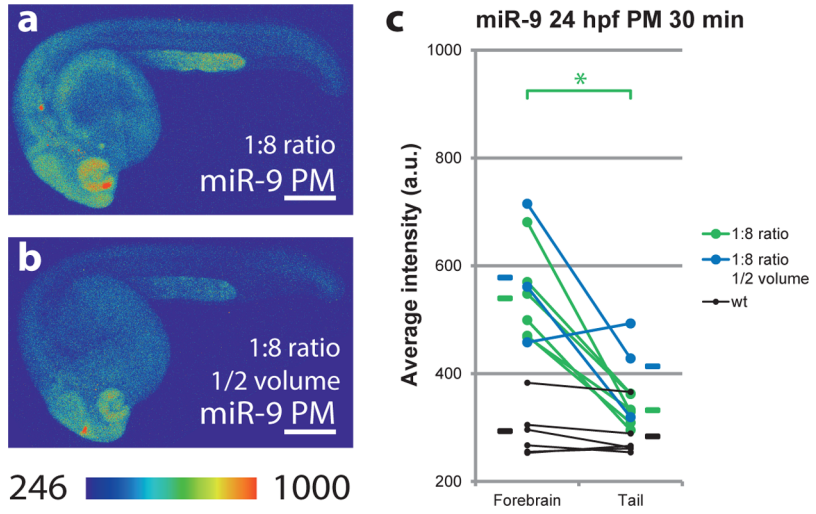

Figure 5. *In vivo* miR-9 templated chemistry at a different probe ratio and quantity. (a) Same conditions as shown in Figure 2k, but with half the concentration of Ru probe ([Ru]:[Rhod] = 1:8). (b) Same conditions as shown in Figure 5a, but with half of the reagents (achieved by injecting 0.5× the volume compared to Figure 5a). (c) Plot of fluorescence intensities measured for each embryo in the forebrain and the tail (black, conditions of Figure 5a; blue, conditions of Figure 5b, locations of fluorescence intensity measurement are indicated in Figure 3f). Average fluorescence intensities are indicated by horizontal bars (one-tailed paired Wilcoxon test; PM (n = 6), MM (n = 3)).

4a, the performance of the reaction is unaffected by the change in reagent concentration down to 25 nM. This is consistent with the fact that the effective concentration of the reagent remains the same on the ternary hybridization complex. Next, we investigated the detection threshold using 30 min irradiation at low reagent concentration (25 nM rhodamine−probe conjugate, 20% ruthenium probe, Figure 4b). A sequence specific and statistically significant increase in fluorescence was measured down to 100 pM concentration of template after 30 min irradiation. While the quantity (number of copies or cellular concentration) of miRNAs has not been reported in zebrafish, extrapolation from human hematopoietic progenitor cells suggests that abundant miRNAs are present at 500−2000 copies per cell[28] which corresponds to low nM concentrations, well within the detection limit of the method.

To test the resilience of the reaction *in vivo*, embryos were injected with a different ratio of the two reagents (rhodamine probe:ruthenium probe of 1:8 rather than 1:4, Figure 5a for a representative image) or with half the injection volume (0.25 nL, 1:8 ratio, Figure 5b for a representative image) according to the aforementioned protocol. Using the same analysis as above, a comparable qualitative difference with a higher fluorescence in the brain than in the tail was observed in 8 out of 9 embryos (Figure 5c). The fact that a comparable result is obtained while reducing probe concentration is consistent with the fact that the probes are in excess relatively to the targeted miRNA. Importantly, it demonstrates that the outcome of *in vivo* templated reactions are tolerant to the inherent small variability in the quantity of administered probes.

In summary, we have described a nucleic acid templated chemical reaction that reports on specific RNA sequences in a live vertebrate thus providing a rapid and simple platform to image miRNA. The reported protocol is dramatically faster than *in situ* methods, which require proteinase K permeabiliza-

DOI: 10.1021/acscentsci.6b00054
ACS Cent. Sci. 2016, 2, 394−400

tion, fixations, and multiple long incubations for reagent hybridization and staining.[23] While several technologies make possible the use of transgenic biosensors to report on nucleic acid localization,[29,30] also in model organisms including zebrafish,[31] this is the first methodology to achieve such detection in a wild-type live animal which does not need to be genetically modified, yielding a higher versatility and simplicity of the method. Furthermore, in the case of mature miRNA, this is the first method for *in vivo* detection. In addition, the ability to translate a specific nucleic acid cue into a chemical reaction can also be used to unmask bioactive molecules. Therefore, the method is applicable beyond the imaging readout demonstrated here, raising the possibility to use this system for theragnostic applications and to redirect biochemical circuitries toward artificial function with the unmasking of an effector molecule. The demonstration that the ruthenium-photocatalyzed azide reduction can be performed in a live vertebrate adds a valuable reaction to the chemical toolbox for *in vivo* chemistry.

■ ASSOCIATED CONTENT

Supporting Information

The Supporting Information is available free of charge on the ACS Publications website at DOI: 10.1021/acscentsci.6b00054.

Sequences of PNA probes, images of zebrafishes, experimental procedures, and physical characterization of the probes (PDF)

■ AUTHOR INFORMATION

Corresponding Authors

*E-mail: Marcos.Gonzalez@unige.ch.
*E-mail: Nicolas.Winssinger@unige.ch.

Author Contributions

L.H. performed the image and data analysis, injected embryos, interpreted data and wrote the paper; I.O. performed the templated chemistry in zebrafish, confocal imaging and interpreted data; M.A. prepared the probes; E.L. performed in vitro templated chemistry; K.-K. S. performed initial experiments with PNA distribution and templated chemistry in vertebrates; M.-G. G. interpreted data and wrote the paper; N.W. conceived the project, interpreted data and wrote the paper.

Notes

The authors declare no competing financial interest.

■ ACKNOWLEDGMENTS

This work was supported by the SNSF (Grant 200020_157106) and the NCCR chemical biology. L.H. is supported by a Marie-Curie Intra-European Fellowship. M.G.-G. is supported by Departement de l'Instruction Publique of the Canton of Geneva, the SNF, the SystemsX epiPhysX program, the ERC (Sara and Morphogen), and the Polish-Swiss research programs. The authors thank Marine Dubois for assistance with molecular biology.

■ REFERENCES

(1) Laughlin, S. T.; Baskin, J. M.; Amacher, S. L.; Bertozzi, C. R. In vivo imaging of membrane-associated glycans in developing zebrafish. *Science* **2008**, *320*, 664−667.

(2) Borrmann, A.; van Hest, J. C. M. Bioorthogonal chemistry in living organisms. *Chem. Sci.* **2014**, *5*, 2123−2134.

(3) Giraldez, A. J.; Cinalli, R. M.; Glasner, M. E.; Enright, A. J.; Thomson, J. M.; Baskerville, S.; Hammond, S. M.; Bartel, D. P.; Schier, A. F. MicroRNAs regulate brain morphogenesis in zebrafish. *Science* **2005**, *308*, 833−838.

(4) Lu, J.; Getz, G.; Miska, E. A.; Alvarez-Saavedra, E.; Lamb, J.; Peck, D.; Sweet-Cordero, A.; Ebert, B. L.; Mak, R. H.; Ferrando, A. A.; Downing, J. R.; Jacks, T.; Horvitz, H. R.; Golub, T. R. MicroRNA expression profiles classify human cancers. *Nature* **2005**, *435*, 834−838.

(5) Winter, J.; Jung, S.; Keller, S.; Gregory, R. I.; Diederichs, S. Many roads to maturity: microRNA biogenesis pathways and their regulation. *Nat. Cell Biol.* **2009**, *11*, 228−234.

(6) Thisse, C.; Thisse, B. High-resolution in situ hybridization to whole-mount zebrafish embryos. *Nat. Protoc.* **2008**, *3*, 59−69.

(7) Tyagi, S.; Kramer, F. R. Molecular beacons: Probes that fluoresce upon hybridization. *Nat. Biotechnol.* **1996**, *14*, 303−308.

(8) Seferos, D. S.; Giljohann, D. A.; Hill, H. D.; Prigodich, A. E.; Mirkin, C. A. Nano-flares: Probes for transfection and mRNA detection in living cells. *J. Am. Chem. Soc.* **2007**, *129*, 15477−15479.

(9) Choi, H. M. T.; Chang, J. Y.; Trinh, L. A.; Padilla, J. E.; Fraser, S. E.; Pierce, N. A. Programmable in situ amplification for multiplexed imaging of mRNA expression. *Nat. Biotechnol.* **2010**, *28*, 1208−1212.

(10) Abe, H.; Kool, E. T. Flow cytometric detection of specific RNAs in native human cells with quenched autoligating FRET probes. *Proc. Natl. Acad. Sci. U. S. A.* **2006**, *103*, 263−268.

(11) Pianowski, Z.; Gorska, K.; Oswald, L.; Merten, C. A.; Winssinger, N. Imaging of mRNA in Live Cells Using Nucleic Acid-Templated Reduction of Azidorhodamine Probes. *J. Am. Chem. Soc.* **2009**, *131*, 6492−6497.

(12) Sadhu, K. K.; Winssinger, N. Detection of miRNA in Live Cells by Using Templated RuII-Catalyzed Unmasking of a Fluorophore. *Chem. - Eur. J.* **2013**, *19*, 8182−8189.

(13) Gorska, K.; Winssinger, N. Reactions Templated by Nucleic Acids: More Ways to Translate Oligonucleotide-Based Instructions into Emerging Function. *Angew. Chem., Int. Ed.* **2013**, *52*, 6820−6843.

(14) Chen, Y. Y.; Kamlet, A. S.; Steinman, J. B.; Liu, D. R. A biomolecule-compatible visible-light-induced azide reduction from a DNA-encoded reaction-discovery system. *Nat. Chem.* **2011**, *3*, 146−153.

(15) Egholm, M.; Buchardt, O.; Christensen, L.; Behrens, C.; Freier, S. M.; Driver, D. A.; Berg, R. H.; Kim, S. K.; Norden, B.; Nielsen, P. E. PNA hybridizes to complementary oligonucleotides obeying the Watson-Crick hydrogen-bonding rules. *Nature* **1993**, *365*, 566−568.

(16) Wienholds, E.; Kloosterman, W. P.; Miska, E.; Alvarez-Saavedra, E.; Berezikov, E.; de Bruijn, E.; Horvitz, H. R.; Kauppinen, S.; Plasterk, R. H. A. MicroRNA expression in zebrafish embryonic development. *Science* **2005**, *309*, 310−311.

(17) Leucht, C.; Stigloher, C.; Wizenmann, A.; Klafke, R.; Folchert, A.; Bally-Cuif, L. MicroRNA-9 directs late organizer activity of the midbrain-hindbrain boundary. *Nat. Neurosci.* **2008**, *11*, 641−648.

(18) Sehm, T.; Sachse, C.; Frenzel, C.; Echeverri, K. miR-196 is an essential early-stage regulator of tail regeneration, upstream of key spinal cord patterning events. *Dev. Biol.* **2009**, *334*, 468−480.

(19) He, X. J.; Yan, Y. L.; Eberhart, J. K.; Herpin, A.; Wagner, T. U.; Schartl, M.; Postlethwait, J. H. miR-196 regulates axial patterning and pectoral appendage initiation. *Dev. Biol.* **2011**, *357*, 463−477.

(20) Kim, H. K.; Lee, Y. S.; Sivaprasad, U.; Malhotra, A.; Dutta, A. Muscle-specific microRNA miR-206 promotes muscle differentiation. *J. Cell Biol.* **2006**, *174*, 677−687.

(21) Stahlhut, C.; Suarez, Y.; Lu, J.; Mishima, Y.; Giraldez, A. J. miR-1 and miR-206 regulate angiogenesis by modulating VegfA expression in zebrafish. *Development* **2012**, *139*, 4356−4364.

(22) Kloosterman, W. P.; Wienholds, E.; de Bruijn, E.; Kauppinen, S.; Plasterk, R. H. A. In situ detection of miRNAs in animal embryos using LNA-modified oligonucleotide probes. *Nat. Methods* **2006**, *3*, 27−29.

(23) Pena, J. T. G.; Sohn-Lee, C.; Rouhanifard, S. H.; Ludwig, J.; Hafner, M.; Mihailovic, A.; Lim, C.; Holoch, D.; Berninger, P.; Zavolan, M.; Tuschl, T. miRNA in situ hybridization in formaldehyde and EDC-fixed tissues. *Nat. Methods* **2009**, *6*, 139−141.

(24) Cheng, C. J.; Bahal, R.; Babar, I. A.; Pincus, Z.; Barrera, F.; Liu, C.; Svoronos, A.; Braddock, D. T.; Glazer, P. M.; Engelman, D. M.;

DOI: 10.1021/acscentsci.6b00054
ACS Cent. Sci. 2016, 2, 394−400

Saltzman, W. M.; Slack, F. J. MicroRNA silencing for cancer therapy targeted to the tumour microenvironment. *Nature* **2015**, *518*, 107−110.
(25) Dragulescu-Andrasi, A.; Rapireddy, S.; Frezza, B. M.; Gayathri, C.; Gil, R. R.; Ly, D. H. A simple gamma-backbone modification preorganizes peptide nucleic acid into a helical structure. *J. Am. Chem. Soc.* **2006**, *128*, 10258−10267.
(26) Yeh, J. I.; Shivachev, B.; Rapireddy, S.; Crawford, M. J.; Gil, R. R.; Du, S. C.; Madrid, M.; Ly, D. H. Crystal Structure of Chiral gamma PNA with Complementary DNA Strand: Insights into the Stability and Specificity of Recognition and Conformational Preorganization. *J. Am. Chem. Soc.* **2010**, *132*, 10717−10727.
(27) Xu, Y.; He, J.; Wang, X.; Lim, T. M.; Gong, Z. Asynchronous activation of 10 muscle-specific protein (MSP) genes during zebrafish somitogenesis. *Dev. Dyn.* **2000**, *219*, 201−215.
(28) Bissels, U.; Wild, S.; Tomiuk, S.; Holste, A.; Hafner, M.; Tuschl, T.; Bosio, A. Absolute quantification of microRNAs by using a universal reference. *RNA* **2009**, *15*, 2375−2384.
(29) Paige, J. S.; Wu, K. Y.; Jaffrey, S. R. RNA Mimics of Green Fluorescent Protein. *Science* **2011**, *333*, 642−646.
(30) Park, H. Y.; Lim, H.; Yoon, Y. J.; Follenzi, A.; Nwokafor, C.; Lopez-Jones, M.; Meng, X. H.; Singer, R. H. Visualization of Dynamics of Single Endogenous mRNA Labeled in Live Mouse. *Science* **2014**, *343*, 422−424.
(31) Campbell, P. D.; Chao, J. A.; Singer, R. H.; Marlow, F. L. Dynamic visualization of transcription and RNA subcellular localization in zebrafish. *Development* **2015**, *142*, 1368−1374.

DOI: 10.1021/acscentsci.6b00054
ACS Cent. Sci. 2016, 2, 394−400